Classical and quantum-linearized descriptions of degenerate optomechanical parametric oscillators

Sebastian Pina-Otey,[1] Fernando Jiménez,[2] Peter Degenfeld-Schonburg,[3] and Carlos Navarrete-Benlloch[1,*]

[1]*Max-Planck-Institut für Quantenoptik, Hans-Kopfermann-strasse 1, 85748 Garching, Germany*

[2]*Zentrum Mathematik der Technische Universität München, Boltzmann-strasse 3, 85747 Garching, Germany*

[3]*Physik Department, Technische Universität München, James Franck Straße, 85748 Garching, Germany*

Recent advances in the development of modern quantum technologies have opened the possibility of studying the interplay between spontaneous parametric down-conversion and optomechanics, two of the most fundamental nonlinear optical processes. Apart from practical reasons, such a scenario is very interesting from a fundamental point of view, because it allows exploration of the optomechanical interaction in the presence of a strongly quantum-correlated field, the spontaneously down-converted mode. In this work we analyze this problem from two approximate but valuable perspectives: the classical limit and the limit of small quantum fluctuations. We show that, in the presence of optomechanical coupling, the well-known classical phase diagram of the optical problem is modified by the appearance of additional dynamical instabilities. As for the quantum-mechanical description, we prove the ability of the squeezed down-converted field to cool down the mechanical motion not only to thermal but also to squeezed thermal mechanical states, and in a way that can be much less sensitive to the parameters (e.g., detuning of the driving laser) than standard sideband cooling.

I. INTRODUCTION

Spontaneous parametric down-conversion is a process which occurs in crystals with second-order optical nonlinearity, where light at some frequency $2\omega_0$ can be transformed into light at frequencies ω_s and ω_i such that $\omega_s + \omega_i \approx 2\omega_0$ [1–4]. When the crystal is introduced in an optical cavity, which has the effect of enhancing the nonlinear interaction and filtering the fields at once, we obtain the so-called optical parametric oscillator (OPO), in which the down-converted field starts oscillating in the cavity only once the power of the pumping laser exceeds some threshold value (such that the nonlinear gain can compensate for the cavity losses) [1,3,4]. These devices have found many applications both in classical and in quantum optics. In the classical case, they are among the most tunable sources of light, allowing us to transform laser light into almost any (optical) frequency [1]. From a quantum point of view, the down-converted photons show strong quantum correlations; particularly relevant to this work is the degenerate optical parametric oscillator (DOPO), in which down-converted photons have the same frequency, $\omega_s = \omega_i \approx \omega_0$, and the corresponding output field shows nearly perfect quadrature squeezing when working close to threshold [2–4]. Indeed, DOPOs are nowadays the sources of the highest quality squeezed light [5–8], which can be used to increase the sensitivity of measurements beyond the standard quantum limit [9–13] or to generate entangled beams for quantum information purposes [14–16].

On the other hand, we have optomechanical systems, where some mechanical degree of freedom is coupled to a light field via, e.g., radiation pressure [17–20]. When the interaction occurs inside a cavity, the Lorentzian density of modes provided by the resonator, together with the injection of a coherent laser field with the proper detuning with respect to the cavity resonance, allows us to cool down the mechanical degree of freedom to its quantum mechanical ground state through sideband cooling [21–33] . Since the mechanical degree of freedom is usually a mesoscopic system formed by many atoms, optomechanics provides a very promising platform where studying the transition from the microscopic quantum world to our natural macroscopic classical one, allowing one, for example, to put bounds on collapse models [34–37]. From a practical point of view, apart from offering a new platform where performing traditional quantum optical tasks such as the generation of squeezed light [38–41], transparency windows [42–46], or photon blockade effects [47], optomechanical systems might be a perfect interface between optical and microwave technologies, since mechanical degrees of freedom couple to both electromagnetic scales [48–57].

As for actual optomechanical implementations, they manifest in many different forms [20]: cavities with mirrors attached to cantilevers [21,22] or in suspension [24], flexible membranes placed inside optical cavities [25,26,29], and localized mechanical modes in photonic crystal cavities [28] are some examples. For our current purposes, the most relevant implementations consist in (i) whispery-gallery-mode resonators (microtoroids and microdisks, for example), where light circulates around its edge via total internal reflection, pushing the whole structure, hence exciting some of its mechanical modes [23,58], and (ii) flexible drum-shaped capacitors coupled to superconducting LC resonators [27,44,59].

From a fundamental point of view, the interplay between optomechanics and down-conversion seems to be a natural and interesting problem to study within the nonlinear quantum optics community. Recent theoretical results for the case in which the down-converted mode is seeded with an external field predict that such a *stimulated* down-conversion process is able to enhance optomechanical cooling [60], normal mode splitting [61], and the sensitivity of mechanical quadrature measurements [62], as well as to generate mechanically squeezed states [63] or even bring the optomechanical interaction to the (single-quantum) strong-coupling regime [64].

*carlos.navarrete@mpq.mpg.de

In the second-harmonic generation configuration (in which only the down-converted frequency is driven), multipartite optomechanical entanglement has also been predicted [65].

Modern platforms capable of combining down-conversion and optomechanics in the same device have transformed the motivation for studying such a scenario into a practical one. In particular, miniaturized whispering-gallery-mode resonators can be fabricated directly with the typical crystalline materials possessing second-order optical nonlinearity, such that light can be down-converted while circulating on the resonator [66–78]. A completely different, but equally realistic implementation could consist of a superconducting circuit in the degenerate parametric oscillation configuration [79] coupled to a drum-shaped capacitor acting as a mechanical degree of freedom [27,44,59] (see also [80] for a recent circuit QED proposal). The third and natural option would consist in using a standard OPO cavity built with a movable micromirror similar to those in [21] and [22].

One of the most relevant questions in these scenarios concerns the effect that the spontaneously down-converted light, which shows strong quantum correlations, will have on the mechanical state. As a step towards understanding this question, in this work we analyze the system from a classical perspective, providing also a small glance at the quantum properties predicted by a linearization of quantum fluctuations around the classical solution. For simplicity, we stick to the degenerate case and assume that only the down-converted field is coupled to the mechanical mode. The latter is a natural situation in circuit setups (where the pump and down-converted modes are provided by different linear circuits) or when the movable mirror is introduced in an OPO that makes use of dual semimonolithic designs [81] (see Fig. 1) to create independent cavities for the pump and down-converted fields;
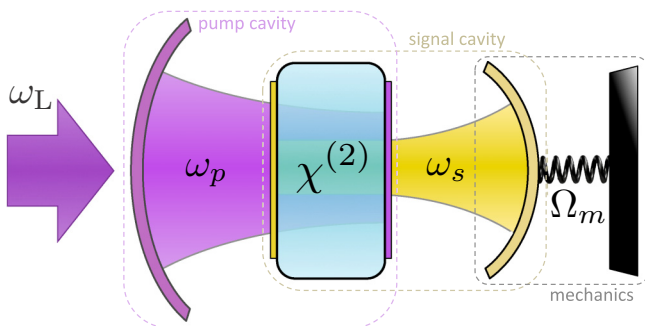

FIG. 1. Sketch of the degenerate optomechanical parametric oscillator considered in this work. It consists of a cavity containing a mode at frequency ω_p (pump) driven by a laser at frequency ω_L. The pump cavity shares a $\chi^{(2)}$ nonlinear crystal with another cavity containing a resonance at frequency ω_s close to $\omega_L/2$ (signal), which can then be populated via degenerate down-conversion of the pumping laser in the crystal. One of the mirrors of the signal cavity is not fixed and can act as a mechanical oscillator forced by the radiation pressure exerted from the light contained in the cavity. OPOs based on dual semimonolithic cavities [81] can implement this exact setup, but other platforms such as crystalline whispering-gallery-mode resonators [66–78] and superconducting circuits [27,44,59,79,80] are already at a point where the model analyzed in our work can be studied experimentally.

in the case of crystalline whispering-gallery-mode resonators it might require choosing a proper mechanical mode weakly coupled to the optical modes around the pump frequency. From a fundamental point of view, this configuration provides probably the most exciting scenario, since the pump stays near-coherent for most of the DOPO parameters, and its coupling to the mechanics could mask the effects generated by the quantum-correlated down-converted field.

Concerning the classical limit, we show that, with respect to the usual DOPO scenario [82–84], the most relevant effect that the optomechanical interaction has is the generation of new dynamical instabilities, as well as the modification of the region of intensity bistability. On the other hand, regarding the quantum-linearized theory, we first argue how it completely fails to capture the physics below threshold, where the optomechanical interaction is purely nonlinear and requires more sophisticated techniques to describe it, which is precisely what we did in a recent work [85]. Nevertheless, the linearized description provides reasonable predictions above threshold, and we use it to show that the down-converted field can have a deep impact on the mechanical state, but very different from that of the standard coherently pumped optomechanical cavity. In particular, we show that it can cool down the mechanical motion in a way less sensitive to parameters (particularly detuning) than the traditional sideband cooling, even generating squeezed thermal mechanical states as the optomechanical interaction is increased. Let us remark that an understanding of the classical phase diagram is instrumental prior to performing a more accurate quantum analysis, as we emphasized in Ref. [85].

The article is organized as follows. First, we introduce the model of the system, which we have called the *degenerate optomechanical parametric oscillator* (DOMPO) and we describe it through a set of quantum Langevin equations. Next, we study the classical limit of the model, finding its steady states and analyzing their stability. Finally, we apply the standard linearization technique to study the quantum properties of the mechanical mode in regions of the parameter space where the classical stationary solution is stable.

II. THE MODEL

Even though the actual implementation can differ from the simple picture sketched in Fig. 1, a DOMPO can be schematically understood as depicted there. Consider a cavity pumped by a laser at frequency ω_L close to one of its resonances ω_p. This cavity (denoted they *pump cavity*) shares a second-order nonlinear crystal with another cavity (the *signal cavity*) in which a resonance ω_s close to $\omega_L/2$ exists and, therefore, can be populated via down-conversion of pump photons in the crystal. Finally, one mirror of the signal cavity can oscillate at frequency Ω_m and then acts as a mechanical oscillator which is forced via the radiation pressure exerted by the signal field.

Let us denote by $\hat{x}_m = \hat{Q}/Q_0$ the displacement of the mirror ($\hat{Q}$) normalized to the zero-point position fluctuations $Q_0 = \sqrt{\hbar/2\Omega_m M}$, where M is the mirror's mass. We also normalize the corresponding momentum $\hat{P}$ to the zero-point momentum fluctuations $P_0 = \hbar/Q_0$, obtaining the normalized momentum $\hat{p}_m = \hat{P}/P_0$. We define annihilation operators $\hat{a}_j$

for pump ($j = $ p) and signal ($j = $ s) photons, with corresponding creation operators $\hat{a}_j^\dagger$. These operators satisfy the commutation relations $[\hat{x}_m, \hat{p}_m] = 2i$ and $[\hat{a}_j, \hat{a}_l^\dagger] = \delta_{jl}$, any other commutator between them being 0. In a picture rotating at the laser frequency ω_L for the pump and $\omega_L/2$ for the signal, the physical processes described in the previous paragraph are then captured by the Hamiltonian $\hat{H} = \hat{H}_O + \hat{H}_M + \hat{H}_{DC} + \hat{H}_{OM}$, with [2–4,20]

$$\hat{H}_O = -\sum_{j=\mathrm{p,s}} \hbar \Delta_j \hat{a}_j^\dagger \hat{a}_j + i\hbar \mathcal{E}_L (\hat{a}_p^\dagger - \hat{a}_p), \tag{1a}$$

$$\hat{H}_M = \frac{\hbar \Omega_m}{4}\left(\hat{x}_m^2 + \hat{p}_m^2\right), \tag{1b}$$

$$\hat{H}_{DC} = i\hbar \chi \left(\hat{a}_p \hat{a}_s^{\dagger 2} - \hat{a}_p^\dagger \hat{a}_s^2\right), \tag{1c}$$

$$\hat{H}_{OM} = -g_s \hat{a}_s^\dagger \hat{a}_s \hat{x}_m, \tag{1d}$$

where $\Delta_p = \omega_L - \omega_p$ and $\Delta_s = \omega_L/2 - \omega_s$ denote the detuning of the laser with respect to the pump and signal modes, $\mathcal{E}_L$ is the pump cavity's driving rate (proportional to the square root of the power of the external laser), χ is the down-conversion rate (proportional to the crystal's nonlinear susceptibility), and g_s is the optomechanical scattering rate (which depends strongly on the particular implementation).

In addition to these coherent processes, the system is subject to incoherent processes. In particular, we need to take into account the loss of photons through the partially transmitting mirrors (open cavities) and the coupling of the mechanical oscillator to its thermal environment, reaching some equilibrium temperature T in the absence of light. We choose to include these processes at the level of the Heisenberg equations of motion, leading to the widely used quantum Langevin equations [86,87]

$$\frac{d\hat{x}_m}{dt} = \Omega_m \hat{p}_m,$$

$$\frac{d\hat{p}_m}{dt} = -\gamma_m \hat{p}_m - \Omega_m \hat{x}_m + 2g_s \hat{a}_s^\dagger \hat{a}_s + \sqrt{4\gamma_m \bar{n}_{th}}\,\hat{p}_{m,in}(t),$$

$$\frac{d\hat{a}_p}{dt} = \mathcal{E}_L - (\gamma_p - i\Delta_p)\hat{a}_p - \frac{\chi}{2}\hat{a}_s^2 + \sqrt{2\gamma_p}\,\hat{a}_{p,in}(t),$$

$$\frac{d\hat{a}_s}{dt} = -(\gamma_s - i\Delta_s - ig_s \hat{x}_m)\hat{a}_s + \chi \hat{a}_p \hat{a}_s^\dagger + \sqrt{2\gamma_s}\,\hat{a}_{s,in}(t), \tag{2}$$

where γ_j are the rates of exchange of excitations of the modes with their corresponding environments, and the input operators have 0 mean, $\langle \hat{a}_{j,in}(t)\rangle = \langle \hat{p}_{m,in}(t)\rangle = 0$, and nonzero two-time correlators,

$$\langle \hat{a}_{j,in}(t)\hat{a}_{j,in}^\dagger(t')\rangle = \langle \hat{p}_{m,in}(t)\hat{p}_{m,in}(t')\rangle = \delta(t - t'), \tag{3}$$

and play the role of the environmental quantum fluctuations driving the system. In this equations we have assumed to be working in the high-temperature limit where the number of phonons at thermal equilibrium can be approximated by $\bar{n}_{th} \approx k_B T/\hbar \Omega_m \gg 1$.

Before studying the equations, it is convenient to make a variable change that will allow us to see how many free parameters they really have. To this aim, we define the

normalized parameters

$$g_{DC} = \frac{\chi}{\sqrt{\gamma_p \gamma_s}}, \quad \sigma = \frac{\chi \mathcal{E}_L}{\gamma_p \gamma_s}, \quad \kappa = \frac{\gamma_p}{\gamma_s},$$

$$\delta_j = \frac{\Delta_j}{\gamma_j}, \quad \gamma = \frac{\gamma_m}{\gamma_s}, \quad \Omega = \frac{\Omega_m}{\gamma_s}, \quad g = \frac{g_s/\gamma_s}{g_{DC}\sqrt{\Omega}}, \tag{4}$$

time $\tau = \gamma_s t$, system operators

$$\hat{b}_s = g_{DC}\hat{a}_s, \quad \hat{b}_p = \sqrt{\kappa}\,g_{DC}\hat{a}_p,$$

$$\hat{p} = \frac{g_{DC}}{\sqrt{\Omega}}\hat{p}_m, \quad \hat{x} = g_{DC}\sqrt{\Omega}\,\hat{x}_m, \tag{5}$$

and input operators

$$\hat{b}_{j,in}(\tau) = \frac{1}{\sqrt{\gamma_s}}\hat{a}_{j,in}(\tau/\gamma_s),$$

$$\hat{p}_{in}(\tau) = \frac{1}{\sqrt{\gamma_s}}\hat{p}_{m,in}(\tau/\gamma_s), \tag{6}$$

which satisfy the same correlators as before [see Eq. (3)], but now with respect to the dimensionless time τ. With these changes, the quantum Langevin equations are transformed into

$$\frac{d\hat{x}}{d\tau} = \Omega^2 \hat{p},$$

$$\frac{d\hat{p}}{d\tau} = -\gamma \hat{p} - \hat{x} + 2g\hat{b}_s^\dagger \hat{b}_s + \sqrt{\frac{4\gamma \bar{n}_{th}}{\Omega}}\,g_{DC}\hat{p}_{in}(\tau),$$

$$\frac{1}{\kappa}\frac{d\hat{b}_p}{d\tau} = \sigma - (1 - i\delta_p)\hat{b}_p - \frac{1}{2}\hat{b}_s^2 + \sqrt{2}g_{DC}\hat{b}_{p,in}(t),$$

$$\frac{d\hat{b}_s}{d\tau} = -(1 - i\delta_s - ig\hat{x})\hat{b}_s + \hat{b}_p \hat{b}_s^\dagger + \sqrt{2}g_{DC}\hat{b}_{s,in}(t). \tag{7}$$

It is interesting to note that g basically provides the ratio between the optomechanical and the down-conversion couplings, and hence, assuming $\sqrt{\Omega}$ to be of order 1, they inform us about which of the two nonlinear processes dominates.

The quantum Langevin equations are nonlinear operator equations, and hence it is a formidable task to obtain results directly from them without further approximations. In the following, we analyze two relevant limits of these equations: the classical limit and the limit of "small" quantum fluctuations.

III. CLASSICAL ANALYSIS

The classical limit of the model is obtained by assuming that all the modes of the system are in a coherent state. Defining the corresponding amplitudes $\beta_j = \langle \hat{b}_j \rangle$, $x = \langle \hat{x}\rangle$, and $p = \langle \hat{p}\rangle$, and taking the expectation value of the quantum Langevin equations, (7), this approximation leads to the classical equations

$$\dot{x} = \Omega^2 p,$$

$$\dot{p} = -\gamma p - x + 2g|\beta_s|^2,$$

$$\kappa^{-1}\dot{\beta}_p = \sigma - (1 - i\delta_p)\beta_p - \beta_s^2/2,$$

$$\dot{\beta}_s = -(1 - i\delta_s - igx)\beta_s + \beta_p \beta_s^*. \tag{8}$$

As these are nontrivial nonlinear equations, it is not possible to find their time-dependent analytical solutions other than
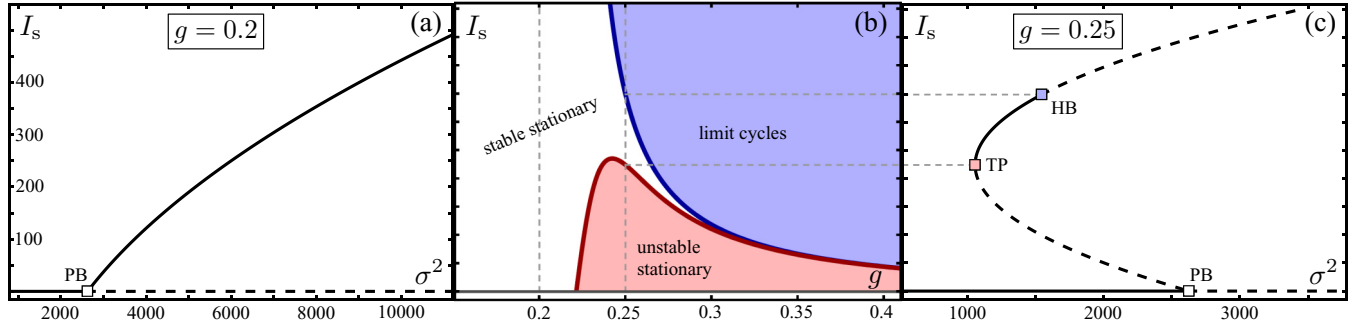
FIG. 2. Bifurcations and corresponding stable and unstable regions for one particular example for which we have chosen $\gamma = 0.005$, $\Omega = -\delta_s = 10$, $\delta_p = 5$, and $\kappa = 100$, the first three being typical parameters when aiming for sideband cooling in optomechanical systems. Note that this fixes all the parameters but g and I_s (we use the steady-state intensity I_s as a parameter instead of σ, because the latter can be uniquely determined from the former but, in general, not the other way around). In (b) we show in the space of these parameters the turning point (thick red line) and the single Hopf instability (thick blue line) found in this example, coloring the regions where they make the stationary solution unstable. Note that for this choice of parameters, in the absence of optomechanical coupling there are no instabilities apart from the trivial pitchfork bifurcation, as can be checked from conditions (14) and (17). Hence, we see that the effect of the optomechanical coupling in this case consists in introducing new instabilities which greatly reduce the domain of stability of the nontrivial stationary state. In (a) and (c) we show how the steady-state intensity I_s depends on the injection σ^2 for two specific values of g, corresponding to the vertical dashed gray lines in the parameter space (b), denoting its unstable and stable regions by dashed and solid lines, respectively. In (a) we have chosen $g = 0.2$, for which no instabilities are present in the nontrivial solution, as can be appreciated in (b), and hence only the pitchfork instability connecting the trivial and nontrivial solutions is present. In (c), on the other hand, we have chosen $g = 0.25$, for which we find both a turning point (and hence a domain of bistability between the trivial and the nontrivial solutions) and a Hopf bifurcation leading to time-dependent asymptotic solutions.

numerically. However, working with a dissipative system, we are mainly interested in its behavior for long times (asymptotic limit), and there is a lot that we can say about this without really solving the full nonlinear equations; in particular, we follow closely the procedure already applied to detuned DOPOs [82–84].

A. Stationary solutions

The simplest asymptotic behavior that one can expect is that the system reaches some steady state. Hence, it is always convenient to start by finding the time-independent solutions to the nonlinear equations, which we denote with a bar, e.g., $\bar{x}$; when needed, we write the complex field amplitudes as $\bar{\beta}_j = \sqrt{I_j} \exp(i\varphi_j)$, with real variables $\varphi_j \in]-\pi,\pi]$ and $I_j \geqslant 0$.

All the stationary solutions of (8) have $\bar{p} = 0$ and $\bar{x} = 2gI_s$, leaving us with

$$\sigma = (1 - i\delta_p)\bar{\beta}_p + \bar{\beta}_s^2/2, \tag{9a}$$

$$\bar{\beta}_p \bar{\beta}_s^* = (1 - i\delta_s - 2ig^2 I_s)\bar{\beta}_s. \tag{9b}$$

We then distinguish two types of stationary solutions: *trivial* or *below-threshold* solutions, which have $I_s = 0$; and *nontrivial* or *above-threshold* solutions, with $I_s \neq 0$.

In the trivial case, the solution is simply

$$\bar{\beta}_s = 0 \quad \text{and} \quad \bar{\beta}_p = \sigma/(1 - i\delta_p). \tag{10}$$

As for the nontrivial solutions, we find their analytic expression as follows. First, note that (9b) implies $\bar{\beta}_p = (1 - i\delta_s - 2ig^2 I_s)e^{2i\varphi_s}$, which, plugged into (9a), leads to $e^{-2i\varphi_s}\sigma = (1 - i\delta_p)(1 - i\delta_s - 2ig^2 I_s) + I_s/2$, whose absolute value squared gives us a second-order polynomial for the signal

intensity,

$$\sigma^2 = \left[1 + \frac{I_s}{2} - \delta_p(\delta_s + 2g^2 I_s)\right]^2 + (\delta_p + \delta_s + 2g^2 I_s)^2$$
$$\equiv q_0 + q_1 I_s + q_2 I_s^2, \tag{11}$$

with

$$q_0 = (1 + \delta_p^2)(1 + \delta_s^2), \tag{12a}$$

$$q_1 = (1 - \delta_p\delta_s) + 4\delta_s(1 + \delta_p^2)g^2, \tag{12b}$$

$$q_2 = 4g^4 + (\tfrac{1}{2} - 2\delta_p g^2)^2. \tag{12c}$$

Depending on the value of the parameters, this equation can have a single real positive solution or two, as shown in Fig. 2. In order to find the values of the parameters (in particular, of the injection σ and the detunings δ_j, experimentally tunable) for which this happens, we just need to obtain the expression for the turning point, labeled "TP" in Fig. 2, which is nothing but the extremum of $\sigma^2(I_s)$, that is,

$$\left.\frac{\partial\sigma^2}{\partial I_s}\right|_{I_s=I_s^{\mathrm{TP}}} = 0 \implies I_s^{\mathrm{TP}} = -q_1/2q_2. \tag{13}$$

Taking into account that $q_2 > 0$, the turning point will exist only if $q_1 < 0$, which gives us a condition on the detunings for a given optomechanical coupling:

$$\delta_p\delta_s > 1 + 4\delta_s(1 + \delta_p^2)g^2. \tag{14}$$

Hence, when this condition is satisfied, we will have two possible steady-state signal intensities (three counting the trivial one) for injections $\sigma^2 \in]q_0 - q_1^2/4q_2, q_0]$ [see Fig. 2(c)]. Let us anticipate, however, that the branch connecting the trivial solution with the upper branch of the nontrivial one is unstable (see Fig. 2), so only two of the three possible solutions

can be observed in real experiments, leading to an intensity bistability common in nonlinear optical systems. Finally, note that condition (14) with $g = 0$ is in agreement with that found for detuned DOPOs [82–84].

B. Linear stability analysis

The existence of a mathematical solution of the nonlinear equations is not enough to ensure its physical reality: it also needs to be stable against perturbations, since in the real world these are unavoidable, and therefore we would never be able to observe the system in the corresponding

solution otherwise. Hence, in the following we proceed to study the stability of the stationary solutions found above.

Let us collect the variables of the system in a vector $\mathbf{b} = \mathrm{col}(x, p, \beta_\mathrm{p}, \beta_\mathrm{p}^*, \beta_\mathrm{s}, \beta_\mathrm{s}^*)$. The stability of a given stationary solution $\bar{\mathbf{b}}$ can be analyzed as follows [88]. We consider small fluctuations around it by writing $\mathbf{b}(t) = \bar{\mathbf{b}} + \delta\mathbf{b}(t)$, introduce this ansatz into the nonlinear system (8), and keep only terms which are linear in the fluctuations, obtaining a linear system $\delta\dot{\mathbf{b}} = \mathcal{L}\delta\mathbf{b}$, where $\mathcal{L}$ is the so-called *linear stability matrix*. This matrix depends on the system parameters and the particular stationary solution whose stability we are considering and, in our case, is given by

$$\mathcal{L} = \begin{pmatrix} 0 & \Omega^2 & 0 & 0 & 0 & 0 \\ -1 & -\gamma & 0 & 0 & 2g\bar{\beta}_\mathrm{s}^* & 2g\bar{\beta}_\mathrm{s} \\ 0 & 0 & -\kappa(1 - i\delta_\mathrm{p}) & 0 & -\kappa\bar{\beta}_\mathrm{s} & 0 \\ 0 & 0 & 0 & -\kappa(1 + i\delta_\mathrm{p}) & 0 & -\kappa\bar{\beta}_\mathrm{s}^* \\ ig\bar{\beta}_\mathrm{s} & 0 & \bar{\beta}_\mathrm{s}^* & 0 & -(1 - i\delta_\mathrm{s} - ig\bar{x}) & \bar{\beta}_\mathrm{p} \\ -ig\bar{\beta}_\mathrm{s}^* & 0 & 0 & \bar{\beta}_\mathrm{s} & \bar{\beta}_\mathrm{p}^* & -(1 + i\delta_\mathrm{s} + ig\bar{x}) \end{pmatrix}. \tag{15}$$

Since the equation for the fluctuations is linear, it is then clear that their dynamical behavior is controlled by the eigenvalues of this matrix. In particular, the fluctuations will be damped and disappear in the asymptotic limit only if the real part of all the eigenvalues is negative. Hence, we say that a stationary solution $\bar{\mathbf{b}}$ is stable (and therefore physical) when all the eigenvalues of its corresponding linear stability matrix $\mathcal{L}(\bar{\mathbf{b}})$ have a negative real part.

The points in the parameter space where at least one of the eigenvalues has 0 real part are known as *critical points*, *instabilities*, or *bifurcations*, and they separate the regions in which the stationary solution changes from stable to unstable. We can distinguish two types of instabilities: *pitchfork* or *static* bifurcations, where the imaginary part of the relevant eigenvalue is also 0, which connect the stationary solution with another stationary solution; and *Hopf* or *dynamic* bifurcations, where the imaginary part of the relevant eigenvalue is nonzero, which connect the stationary solution with a time-dependent solution (usually some periodic solution, known in this context as a *periodic orbit* or *limit cycle*).

Before proceeding, let us comment on one subtle point concerning the system parameters. The linear stability matrix, (15), does not depend explicitly on the injection σ, it does only implicitly, through the intracavity stationary amplitudes $\bar{\beta}_\mathrm{p}$ and $\bar{\beta}_\mathrm{s}$. It is then convenient to use either I_p or I_s as a parameter instead of σ when dealing with the trivial or nontrivial solutions, respectively, knowing that σ can always be uniquely determined from them by using (10) or (11).

Let us now proceed to discuss the instabilities that can be found in the DOMPO. We provide a summary of the main results here and leave the detailed derivations for Appendix A. Concerning the trivial solution, it possesses only one bifurcation, appearing when $I_\mathrm{p} = 1 + \delta_\mathrm{s}^2$. The trivial solution becomes unstable for $I_\mathrm{p} > 1 + \delta_\mathrm{s}^2$ or, in terms of the injection, when $\sigma^2 > (1 + \delta_\mathrm{s}^2)(1 + \delta_\mathrm{p}^2)$. Note that this is precisely the

point at which the trivial and nontrivial solutions coalesce (see points labeled "PB" in Fig. 2), and hence this pitchfork bifurcation simply connects these two stationary solutions. As for the nontrivial solution, it provides one more static instability, at $I_\mathrm{s} = I_\mathrm{s}^\mathrm{TP}$. Hence, we see that the turning point of the nontrivial solution is an instability, and it is simple to check that the lower branch of the nontrivial solution connecting the upper branch with the trivial solution is unstable (for example, by evaluating the eigenvalues numerically for one set of parameters), as shown in Fig. 2. In other words, the turning point is a pitchfork bifurcation connecting the unstable lower branch with the upper branch, which is stable in all its domain of existence, except for possible Hopf bifurcations, which we discuss next. The behavior of the dynamical instabilities of the nontrivial solution is very rich in the DOMPO. Let us first note that in the absence of optomechanical coupling ($g = 0$) there is a single Hopf bifurcation, located at (see Appendix A and [82–84])

$$I_\mathrm{s}^\mathrm{HB} = -\frac{\left(1 + \delta_\mathrm{p}^2\right)\left[(2 + \kappa)^2 + \kappa^2\delta_\mathrm{p}^2\right]}{(1 + \kappa)^2\left(2 + \kappa + \kappa\delta_\mathrm{p}^2 + 2\delta_\mathrm{p}\delta_\mathrm{s}\right)}, \tag{16}$$

which requires

$$\delta_\mathrm{p}\delta_\mathrm{s} < -1 - \kappa\left(1 + \delta_\mathrm{p}^2\right)/2 \tag{17}$$

to exist (otherwise, $I_\mathrm{s}^\mathrm{HB} < 0$), which incidentally means that it does not exist when there is bistability in the system (which requires $\delta_\mathrm{p}\delta_\mathrm{s} > 1$). It is possible to show that the portion of the nontrivial solution with $I_\mathrm{s} > I_\mathrm{s}^\mathrm{HB}$ becomes unstable, and the limit cycles become chaotic for large enough injections [82–84]. The main effect of optomechanics, that is, of increasing g, is both changing the location of this dynamical instability already present for $g = 0$ and creating new ones that cannot be understood as a deformation of the latter. This is what we show in Fig. 2(b) for one example, where we plot

the signal intensity of the Hopf instability that we have found as a function of g. Let us remark that in the $g \neq 0$ case the complicated form of the linear stability matrix has prevented us from finding simple analytic expressions for such instabilities, but we have been able to find a simple way to compute them efficiently with the help of symbolic programs that has allowed us to perform an exhaustive analysis (see Appendix A).

IV. QUANTUM PROPERTIES WITHIN THE LINEARIZED DESCRIPTION

In order to characterize the quantum properties of the DOMPO, we now apply the widely used method of standard linearization [89–92]. In this approach, one assumes that the asymptotic classical solution of the system is a strong attractor, and hence quantum mechanics acts just as strongly damped fluctuations or noise driving the system continuously and trying to bring it out of equilibrium. As we did in the classical analysis, let us collect the fundamental operators of the system into a vector, $\hat{\mathbf{b}} = \text{col}(\hat{x}, \hat{p}, \hat{b}_{\mathrm{p}}, \hat{b}_{\mathrm{p}}^{\dagger}, \hat{b}_{\mathrm{s}}, \hat{b}_{\mathrm{s}}^{\dagger})$. In this scenario, it is then convenient to write the operators as $\hat{\mathbf{b}}(\tau) = \bar{\mathbf{b}} + \delta \hat{\mathbf{b}}(\tau)$, where we remember that $\bar{\mathbf{b}}$ is the stationary solution found for the operators within the classical description of the system (we do not consider periodic orbits in this work, although they can also be studied using a similar approach). Assuming that $\bar{\mathbf{b}}$ is a strong classical attractor, that is, that the eigenvalues of its associated linear stability matrix $\mathcal{L}$ are large enough for quantum fluctuations to be strongly damped, one can neglect terms of the quantum Langevin equations, (7), beyond linear order in the fluctuations $\delta \hat{\mathbf{b}}$, turning them into the linear system

$$\frac{d}{d\tau} \delta \hat{\mathbf{b}} = \mathcal{L} \delta \hat{\mathbf{b}} + \sqrt{2} g_{\mathrm{DC}} \hat{\mathbf{f}}(\tau), \tag{18}$$

where we have defined the input-vector operator

$$\hat{\mathbf{f}}(\tau) = \text{col}\left(0, \sqrt{\frac{2\gamma \bar{n}_{\mathrm{th}}}{\Omega}} \hat{p}_{\mathrm{in}}, \hat{b}_{\mathrm{p,in}}, \hat{b}_{\mathrm{p,in}}^{\dagger}, \hat{b}_{\mathrm{s,in}}, \hat{b}_{\mathrm{s,in}}^{\dagger}\right), \tag{19}$$

which acts precisely as a quantum force continuously driving the system out of equilibrium. Note that the two-time input correlators can be written in the compact form $\langle \hat{f}_j(\tau) \hat{f}_l(\tau') \rangle = M_{jl}\delta(\tau - \tau')$, where M_{jl} are the elements of the matrix $\mathcal{M} = \mathcal{M}_{\mathrm{m}} \oplus \mathcal{M}_{\mathrm{p}} \oplus \mathcal{M}_{\mathrm{s}}$ with

$$\mathcal{M}_{\mathrm{m}} = \begin{pmatrix} 0 & 0 \\ 0 & 2\gamma \bar{n}_{\mathrm{th}}/\Omega \end{pmatrix},$$

$$\mathcal{M}_{\mathrm{p}} = \begin{pmatrix} 0 & \kappa \\ 0 & 0 \end{pmatrix}, \tag{20}$$

$$\mathcal{M}_{\mathrm{s}} = \begin{pmatrix} 0 & 1 \\ 0 & 0 \end{pmatrix}.$$

In the following, we particularize these linearized quantum Langevin equations to the two types of classical stable stationary solutions that we have found (trivial and nontrivial), analyzing the behavior that they predict for the mechanical mode. From the previous discussion, it is clear that such a linearized description will break down close to the critical points of the classical theory, but as proven again and again in many nonlinear optical systems, its predictions usually provide the correct tendency of observables as one approaches the critical points, at the very least qualitatively. There are some exceptions, however, corresponding to cases in which the quantum mechanical effects are purely nonlinear, so that linearization completely misses them. Indeed, we present one such example now.

A. Failure of the method below threshold

The first interesting thing to note about the linearization approach is how it completely fails to capture any optomechanical phenomena that might be occurring below threshold, that is, when the signal field is switched off classically, so that there is no coherent background in the mechanical and signal modes. This is clearly seen from the fact that, as we show in Sec. 1 of Appendix A, the linear stability matrix is written as the direct sum of matrices acting on each mode, so that the equations for the mechanical fluctuations $\delta \hat{x} = \hat{x}$ and $\delta \hat{p} = \hat{p}$ simply read

$$\frac{d\hat{x}}{d\tau} = \Omega^2 \hat{p}, \tag{21a}$$

$$\frac{d\hat{p}}{d\tau} = -\gamma \hat{p} - \hat{x} + \sqrt{\frac{4\gamma \bar{n}_{\mathrm{th}}}{\Omega}} g_{\mathrm{DC}} \hat{p}_{\mathrm{in}}(\tau). \tag{21b}$$

These equations receive absolutely no information from the optical modes, in particular, corresponding to a harmonic oscillator in thermal equilibrium with its environment. In the same way, the fluctuations of the optical mode $\delta \hat{b}_{\mathrm{s}} = \hat{b}_{\mathrm{s}}$ are completely unaffected by the mechanics, since they obey the usual below-threshold DOPO dynamics,

$$\frac{d\hat{b}_{\mathrm{s}}}{d\tau} = (-1 + i\delta_{\mathrm{s}})\hat{b}_{\mathrm{s}} + \bar{\beta}_{\mathrm{p}}\hat{b}_{\mathrm{s}}^{\dagger} + \sqrt{2} g_{\mathrm{DC}} \hat{b}_{\mathrm{s,in}}(\tau). \tag{22}$$

As is well known [2,3,86], the latter equations predict that the signal mode gets more and more squeezed as the critical point of the below-threshold solution $I_{\mathrm{p}} = 1 + \delta_{\mathrm{s}}^2$ is approached, denoted PB in Figs. 2(a) and 2(c). In fact, the linearized description predicts an infinite photon number exactly at threshold [90–92], which of course gets regularized once more accurate approaches are used [89,93–101]. In the light of this insight, it is hard to believe that, despite the large number of photons present in the signal mode, optomechanical scattering will have no effect whatsoever on the fluctuations of the modes, as Eqs. (21) and (22) predict, and one has to conclude that the linearization simply fails to capture whatever phenomena occur below threshold. In fact, in this regime the signal photons scattered by the mechanical mode are purely quantum mechanical, with no coherent or classical background, and this is precisely what makes the optomechanical interaction $\hat{a}_{\mathrm{s}}^{\dagger}\hat{a}_{\mathrm{s}}\hat{x}_{\mathrm{m}}$ purely nonlinear or *non-Gaussian*, which is ultimately the reason why any effect related to it is completely lost upon linearization.

More sophisticated linearized descriptions such as the self-consistent linearization introduced in [89] cannot work either, since it is equivalent to making a Gaussian ansatz for the full state of the system, while the optomechanical interaction becomes purely non-Gaussian below threshold as we have argued above. Hence, more elaborate techniques are required below threshold, such as a numerical simulation based on the

positive P representation [4,93–95,102] or the self-consistent Mori projector operator (c-MoP) theory [101,103], which are beyond the scope of this work, and we indeed explore in other works [85]. Nevertheless, as we are about to see, standard linearization can still be a useful tool, allowing us to analyze the system above threshold and find indications of interesting phenomena.

B. Above-threshold predictions

The situation is rather different above threshold. In this case all the modes have a classical background, and hence it is possible to linearize the optomechanical interaction without losing it completely. Consequently, it is to be expected that, even though the method will fail at the critical points of the classical theory, it will provide us with a good qualitative picture of the trend that the quantum properties of the system follow.

As explained above, the linearization method is equivalent to making a Gaussian ansatz [14–16] for the state of the quantum fluctuations around the classical solution [89,101]. Hence, within this approach the quantum properties of the system are completely characterized by the covariance matrix of all the modes [14–16]. Given the position $\hat{x}_j = \hat{a}_j^\dagger + \hat{a}_j$ and momentum $\hat{p}_j = i(\hat{a}_j^\dagger - \hat{a}_j)$ quadratures of the optical modes ($j =$ p,s) and defining the quadrature vector operator $\hat{\mathbf{r}} = \mathrm{col}(\hat{x}_\mathrm{m}, \hat{p}_\mathrm{m}, \hat{x}_\mathrm{p}, \hat{p}_\mathrm{p}, \hat{x}_\mathrm{s}, \hat{p}_\mathrm{s})$, the covariance matrix V is defined as the symmetric matrix with elements $V_{jl} = \langle \delta\hat{r}_j \delta\hat{r}_l + \delta\hat{r}_l \delta\hat{r}_j \rangle / 2$ [14–16]. In Appendix B we explain how this object can be efficiently evaluated numerically for any value of the parameters directly from the linearized Langevin equations, (18), specifically from the eigensystem of the linear stability matrix, (15).

On the other hand, as explained in Sec. I, the main question that we would like to explore is the effect that the optomechanical interaction has on the mechanical state. In the following we show through a set of examples how the squeezed down-converted field is able to cool down the mechanical motion. Moreover, it does so in a way that can be much less sensitive to parameters than standard sideband cooling. Furthermore, apart from cooling it, the example will show a trend of the optomechanical interaction to squeeze the thermal mechanical motion.

In order to show this, we first find the reduced state of the mechanical mode. Since within the linearized picture the state of the whole system is Gaussian, the reduced mechanical state is Gaussian as well, with a covariance matrix given by the corresponding submatrix of the full covariance matrix, (B4) [16]:

$$V_\mathrm{m} = \begin{pmatrix} V_{11} & V_{12} \\ V_{21} & V_{22} \end{pmatrix}. \tag{23}$$

In order to get a better physical picture of the mechanical state, we further exploit the fact that any single-mode Gaussian state can be written as a squeezed thermal state up to a rotation in phase space [15,16] (which simply provides the direction of phase space along which squeezing occurs). This means that the mechanical state $\hat{\rho}_\mathrm{m}$ can be written in the form

$$\hat{R}(\theta)\hat{\rho}_\mathrm{m}\hat{R}^\dagger(\theta) = \hat{S}(r_\mathrm{eff})\hat{\rho}_\mathrm{th}(\bar{n}_\mathrm{eff})\hat{S}^\dagger(r_\mathrm{eff}) \equiv \tilde{\rho}_\mathrm{m}, \tag{24}$$

for some phase-shift operator $\hat{R}(\theta) = \exp[i\theta(\hat{x}_\mathrm{m}^2 + \hat{p}_\mathrm{m}^2)/4]$, where $\hat{\rho}_\mathrm{th}(\bar{n}_\mathrm{eff})$ is a thermal state with effective phonon number $\bar{n}_\mathrm{eff}$, and $\hat{S}(r_\mathrm{eff}) = \exp[ir_\mathrm{eff}\hat{x}_\mathrm{m}\hat{p}_\mathrm{m}/2]$ is a squeezing operator with effective squeezing parameter r_eff. We are, in particular, interested in the effective phonon number $\bar{n}_\mathrm{eff}$ and the effective mechanical squeezing e^{-2r_eff}, which can be written in terms of
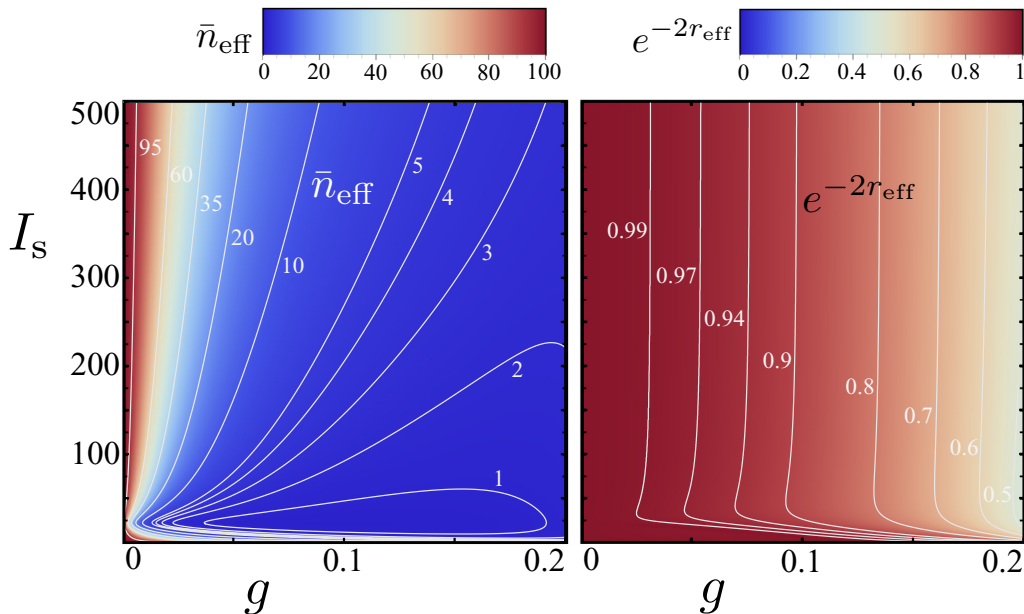

FIG. 3. Density plots of the effective phonon number $\bar{n}_\mathrm{eff}$ and mechanical squeezing e^{-2r_eff} as a function of the optomechanical coupling g and the intracavity signal intensity I_s. The rest of the parameters have the same values as in Fig. 2, and we assume a phonon number $\bar{n}_\mathrm{th} = 100$ at thermal equilibrium. Note how the mechanical state is strongly affected by the optomechanical interaction, which allows both for cooling and for squeezing of the mechanical motion.
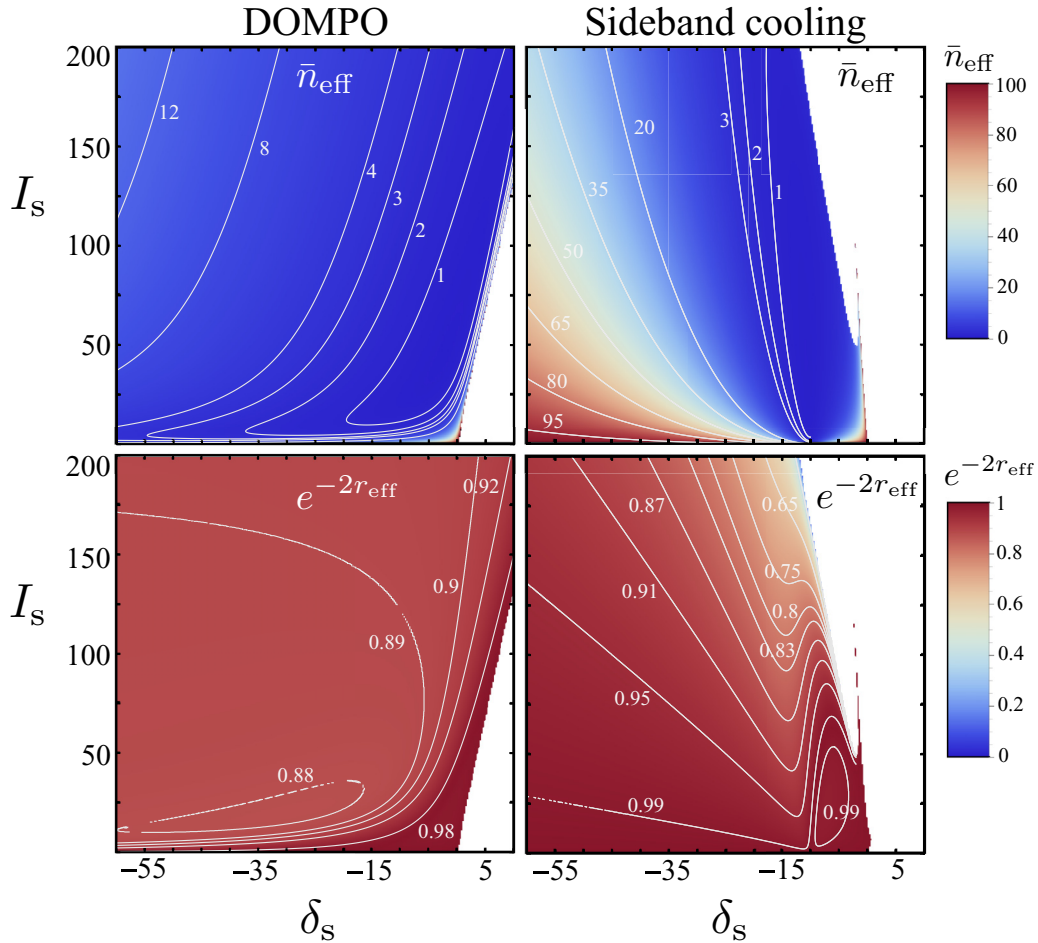
FIG. 4. Density plots of the effective phonon number $\bar{n}_{\text{eff}}$ and mechanical squeezing $e^{-2r_{\text{eff}}}$ as a function of the signal detuning δ_{s} and intensity I_{s}. The rest of the parameters have the same values as in Fig. 3, and we have fixed the optomechanical coupling to $g = 0.1$. Left panels correspond to the DOMPO; right panels, to standard sideband cooling. It is to be appreciated how very insensitive the cooling obtained in the DOMPO is to the detuning, which has to be approximately fixed at $-\Omega$ (red sideband) in a standard sideband-cooling scenario. Note that the white regions correspond to areas of the parameter space where the classical stationary solution is unstable, and hence linearization cannot be applied.

the elements of the covariance matrix as (see Appendix B)

$$\bar{n}_{\text{eff}} = (\sqrt{V_+ V_-} - 1)/2 \quad \text{and} \quad e^{-2r_{\text{eff}}} = \sqrt{V_-/V_+}, \quad (25)$$

where $V_{\mp} = \text{tr}\{V_{\text{m}}\}/2 \mp \sqrt{\text{tr}\{V_{\text{m}}\}^2/4 - \det\{V_{\text{m}}\}}$ are the eigenvalues of the mechanical covariance matrix. Let us now analyze these parameters for a specific situation.

We take as an example the parameters in Fig. 2, for which we have already presented the stable and unstable regions of the classical stationary solution. In Fig. 3 we show the variation of the effective thermal phonon number $\bar{n}_{\text{eff}}$ and squeezing $e^{-2r_{\text{eff}}}$ with g, as we move above threshold, that is, $I_{\text{s}} > 0$. It can be appreciated how the mechanical state is deeply affected by the optomechanical interaction. In particular, we see that the effective phonon number can decrease to low values, which shows the ability of the down-converted field to cool down the mechanical motion. Moreover, as the optomechanical coupling is enhanced, the effective squeezing levels of the thermal mechanical state increase, up to about 50% squeezing in the figure. This opens the possibility of using the DOMPO to generate squeezed mechanical states.

In Fig. 4 we compare the cooling obtained in our system with the cooling that would be obtained in a standard sideband cooling scenario. In particular, for a fixed optomechanical coupling g, we show $\bar{n}_{\text{eff}}$ and $e^{-2r_{\text{eff}}}$ as a function of the signal detuning δ_{s} and I_{s}, for both the DOMPO and standard sideband cooling. We have studied the latter case by considering the standard scenario, consisting of a single driven optical mode interacting with the mechanics, described by the (normalized) quantum Langevin equations

$$\frac{d\hat{x}}{d\tau} = \Omega^2 \hat{p},$$

$$\frac{d\hat{p}}{d\tau} = -\gamma \hat{p} - \hat{x} + 2g\hat{b}_{\text{s}}^{\dagger} \hat{b}_{\text{s}} + \sqrt{\frac{4\gamma \bar{n}_{\text{th}}}{\Omega}} g_{\text{DC}} \hat{p}_{\text{in}}(\tau),$$

$$\frac{d\hat{b}_{\text{s}}}{d\tau} = E - (1 - i\delta_{\text{s}} - ig\hat{x})\hat{b}_{\text{s}} + \sqrt{2} g_{\text{DC}} \hat{b}_{\text{s,in}}(t), \quad (26)$$

where E is the (normalized) amplitude associated with the laser which drives the optical mode. Note that g_{DC} appears here just because we are using the same normalization as in the rest of the paper [see Eqs. (5)], which is convenient for the sake

of comparison; in any case, the final results are independent of this parameter, as can be appreciated from the form of the covariance matrix in Eq. (B4). Collecting the relevant operators in the vector $\hat{\mathbf{b}} = \text{col}(\hat{x},\hat{p},\hat{b}_{\mathrm{s}},\hat{b}_{\mathrm{s}}^{\dagger})$, these equations take the linearized form, (18), with a noise term $\widehat{\mathbf{f}}(\tau)$ without the pump components, and with a linear stability matrix

$$\mathcal{L} = \begin{pmatrix} 0 & \Omega^2 & 0 & 0 \\ -1 & -\gamma & 2g\bar{\beta}_{\mathrm{s}}^* & 2g\bar{\beta}_{\mathrm{s}} \\ ig\bar{\beta}_{\mathrm{s}} & 0 & -(1-i\delta_{\mathrm{s}}-ig\bar{x}) & 0 \\ -ig\bar{\beta}_{\mathrm{s}}^* & 0 & 0 & -(1+i\delta_{\mathrm{s}}+ig\bar{x}) \end{pmatrix},$$

(27)

which is the usual one found in the standard optomechanical case [32,33]. Following the approach explained above, we obtain the covariance matrix, (B4), associated with this problem and, from it, the effective thermal phonon number and effective mechanical squeezing.

The differences in the cooling performance for these two systems can be appreciated in Fig. 4. In particular, it is apparent that the cooling obtained in the DOMPO is less sensitive to the detuning, which in standard sideband cooling needs to be tuned to the red sideband $\delta_{\mathrm{s}} \approx -\Omega$. This insensitivity to the system parameters is something that we have also observed for other parameters and in other regions of the parameter space, and it constitutes a main difference between the DOMPO and standard sideband optomechanical cooling.

V. CONCLUSIONS AND OUTLOOK

In conclusion, in this work we have analyzed the DOMPO from two approximate (but relevant) perspectives: the classical limit and the linearized theory of quantum fluctuations. From a fundamental point of view, this study has been motivated by the question, How does a quantum-correlated field affect the mechanical motion? From a practical viewpoint, the study is timely because it is to be expected that the analyzed model will be experimentally implemented soon, in particular, in the form of crystalline whispering-gallery-mode resonators or superconducting circuits.

We have made an exhaustive analysis of the classical phase diagram, which provides highly relevant information prior to the application of more accurate quantum techniques (see [85] for an example in this direction). Our results show that the optomechanical interaction has the effect of introducing new dynamical instabilities not present in the DOPO, as well as changing the location of the instabilities already present in it.

As for the quantum properties, when working above threshold the linearized theory has shown the ability of the quantum-correlated (squeezed) field to cool down the mechanical motion, not only to a regular thermal state, but also to a squeezed thermal state as the optomechanical coupling is enhanced. Moreover, such cooling has been shown to be more insensitive to the parameters (most prominently detuning) than the one obtained through standard sideband cooling. Unfortunately, in the three-mode problem defined by the DOMPO it is very challenging to get analytical results from the linearization technique or even to get a conclusive physical picture of the observed phenomenology. Therefore, it will

be interesting to apply other techniques which might clarify the physical processes underlying the results presented here. Techniques such as the adiabatic elimination of the optical modes in the master equation of the system might be key to this purpose.

Finally, we emphasize again the failure of the linearization theory below threshold, where the optomechanical interaction becomes purely nonlinear. This opens an even more interesting venue, since it is a problem which will require more elaborate techniques capable of capturing non-Gaussian effects. Particularly relevant for us is the c-MoP theory [103] that we recently applied to the DOPO problem [101], which also has the virtue of regularizing the results at the critical points of the classical theory. With the help of this approach we showed in a recent work [85] that, even below threshold, the down-converted field can cool down the mechanical motion, through a process that we identified by a "cooling by heating" mechanism [104]. It will thus be interesting to analyze whether this is also the mechanism responsible for the cooling that we observe above threshold in this work.

APPENDIX A: DETAILS OF THE STABILITY ANALYSIS OF THE CLASSICAL SOLUTIONS

We provide in this Appendix all the details concerning our treatment of the instabilities present in the DOMPO model, which we summarize in Sec. III B.

1. Stability of the trivial solution

In the case of the trivial stationary solution ($\bar{\beta}_{\mathrm{s}} = 0$), the linear stability matrix, (15), is highly simplified, acquiring, in particular, a box structure $\mathcal{L} = \mathcal{L}_{\mathrm{m}} \oplus \mathcal{L}_{\mathrm{p}} \oplus \mathcal{L}_{\mathrm{s}}$, where the second block is already in diagonal form,

$$\mathcal{L}_{\mathrm{p}} = \begin{pmatrix} -\kappa(1-i\delta_{\mathrm{p}}) & 0 \\ 0 & -\kappa(1+i\delta_{\mathrm{p}}) \end{pmatrix}, \qquad \text{(A1)}$$

and its two eigenvalues have negative real part; the first block is given by

$$\mathcal{L}_{\mathrm{m}} = \begin{pmatrix} 0 & \Omega^2 \\ -1 & -\gamma \end{pmatrix}, \qquad \text{(A2)}$$

whose eigenvalues $\lambda_{\mathrm{m}}^{(\pm)} = -(\gamma \pm \sqrt{\gamma^2 - 4\Omega^2})/2$ also have negative real part, and finally, the last block reads

$$\mathcal{L}_{\mathrm{s}} = \begin{pmatrix} -1 + i\delta_{\mathrm{s}} & \bar{\beta}_{\mathrm{p}} \\ \bar{\beta}_{\mathrm{p}}^* & -1 - i\delta_{\mathrm{s}} \end{pmatrix}, \qquad \text{(A3)}$$

with eigenvalues

$$\lambda_{\mathrm{s}}^{(\pm)} = -1 \pm \sqrt{I_{\mathrm{p}} - \delta_{\mathrm{s}}^2}. \qquad \text{(A4)}$$

Hence, as commented in the text, we see that $\lambda_{\mathrm{s}}^{(+)}$ provides a static instability of the trivial solution, located at $I_{\mathrm{p}} = 1 + \delta_{\mathrm{s}}^2$.

2. Stability of the nontrivial solution

In the case of the nontrivial solution the 6×6 linear stability matrix, (15), does not have a box structure, and hence the eigenvalues do not have simple analytic expressions. However, we are not as interested in the actual eigenvalues as we are in the points where the real part of some of them becomes 0, since these are the points marking the instabilities, and these points can be found by analyzing the characteristic polynomial of the stability matrix, which we write as $P(\lambda) = \sum_{n=0}^{6} c_n \lambda^n$. Most of the coefficients $c_n(I_{\mathrm{s}}, \delta_{\mathrm{s}}, \delta_{\mathrm{p}}, g, \kappa, \gamma, \Omega)$ are quite lengthy, and hence we do not show them here, except for the independent one, which can be written as $c_0 = 4q_2 I_{\mathrm{s}} + 2q_1$, where q_1 and q_2 are defined in (12).

Given the characteristic polynomial, the static instabilities can be found from the condition $P(\lambda = 0) = 0$; that is, they are located in the region of the parameter space defined by the equation $c_0 = 0$, which in our case gives $I_{\mathrm{s}} = I_{\mathrm{s}}^{\mathrm{TP}}$ as mentioned in the text. We can then try to do the same with the Hopf bifurcations, but in that case the expressions are not as easy to handle. It is instructive to first consider the case without optomechanical coupling, $g = 0$. In this case the characteristic polynomial can be factorized as $P(\lambda) = P_{\mathrm{DOPO}}(\lambda) P_{\mathrm{m}}(\lambda)$, where $P_{\mathrm{m}}(\lambda) = \lambda^2 + \gamma\lambda + \Omega^2$ is the characteristic polynomial associated with the free mechanical motion (hence showing no instabilities), while $P_{\mathrm{DOPO}}(\lambda) = \sum_{n=0}^{4} d_n \lambda^n$, with

$$\begin{aligned} d_0 &= \kappa^2 I_{\mathrm{s}}(I_{\mathrm{s}} + 2 - 2\delta_{\mathrm{p}}\delta_{\mathrm{s}}), \\ d_1 &= 2\kappa[I_{\mathrm{s}} + \kappa(1 + I_{\mathrm{s}} + \delta_{\mathrm{p}}^2)], \\ d_2 &= \kappa[4 + 2I_{\mathrm{s}} + \kappa(1 + \delta_{\mathrm{p}}^2)], \\ d_3 &= 2(1 + \kappa), \\ d_4 &= 1, \end{aligned} \qquad \text{(A5)}$$

is the characteristic polynomial associated with the optical modes coupled through the parametric down-conversion process, that is, to the DOPO [82–84]. The Hopf instabilities are found by locating the points in the parameter space where the eigenvalues become purely imaginary, $\lambda = i\omega_{\mathrm{HB}}$, where the real parameter ω_{HB} is known as the *Hopf frequency* (providing the frequency of the periodic solution which is born right at the bifurcation). Applying this condition to the DOPO's characteristic polynomial, we get

$$\begin{aligned} P_{\mathrm{DOPO}}(\lambda = i\omega_{\mathrm{HB}}) &= \left(d_0 - d_2\omega_{\mathrm{HB}}^2 + d_4\omega_{\mathrm{HB}}^4\right) \\ &\quad + i\omega_{\mathrm{HB}}\left(d_1 - d_3\omega_{\mathrm{HB}}^2\right) = 0; \quad \text{(A6)} \end{aligned}$$

the imaginary part of this equation provides us with the Hopf frequency

$$\omega_{\mathrm{HB}}^2 = \frac{d_1}{d_3} = \frac{\kappa[I_{\mathrm{s}} + \kappa(1 + I_{\mathrm{s}} + \delta_{\mathrm{p}}^2)]}{1 + \kappa}, \qquad \text{(A7)}$$

which is well defined for every value of the parameters, while the real part of (A6) provides the condition $d_0 d_3^2 + d_4 d_1^2 - d_2 d_1 d_3 = 0$, which can be solved for I_{s} analytically, leading to the simple expression of Eq. (16) provided in the text.

In the $g \neq 0$ case the large order of the characteristic polynomial has prevented us from finding simple analytic expressions for the dynamical instabilities of the DOMPO. Let us thus explain how we have dealt with them. Proceeding as in the previous case, the real and imaginary parts of $P(\lambda = i\omega_{\mathrm{HB}})$ provide us with two coupled equations:

$$c_0 - c_2\omega_{\mathrm{HB}}^2 + c_4\omega_{\mathrm{HB}}^4 - c_6\omega_{\mathrm{HB}}^6 = 0, \qquad \text{(A8a)}$$

$$\omega_{\mathrm{HB}}\left(c_1 - c_3\omega_{\mathrm{HB}}^2 + c_5\omega_{\mathrm{HB}}^4\right) = 0. \qquad \text{(A8b)}$$

We can see that $\omega_{\mathrm{HB}} = 0$ and $c_0 = 0$ is a solution of the equations, that is, they contain the pitchfork bifurcation, which is not surprising since they are general and valid for any type of instability. Now, for $\omega_{\mathrm{HB}} \neq 0$, we can proceed as follows. The second equation, (A8b), can be solved for the Hopf frequency as

$$\omega_{\mathrm{HB},\pm}^2 = \frac{c_3 \pm \sqrt{c_3^2 - 4c_1 c_5}}{2c_5}; \qquad \text{(A9)}$$

these solutions can be introduced into (A8a), but unfortunately, the resulting equations do not allow us to find a simple analytic solution for I_{s}. However, a symbolic program such as Mathematica allows us to find analytic solutions, provided that we write the equation as a more manageable polynomial. In particular, let us write $\omega_{\mathrm{HB},\pm}^2 = l \pm r$ with $l = c_3/2c_5$ and $r = \sqrt{c_3^2 - 4c_1 c_5}/2c_5$, which allows us to rewrite (A8a) as

$$\begin{aligned} c_0 - c_2 l &+ c_4(l^2 + r^2) - c_6(l^3 + 3lr^2) \\ &= \pm r[c_2 - 2c_4 l + c_6(3l^2 + r^2)]. \quad \text{(A10)} \end{aligned}$$

The square of this expression provides a sixth-order polynomial equation for I_{s}, whose solutions can be efficiently handled by a symbolic program. Note that by taking the square of the previous equation, we are indeed introducing extra fictitious solutions for I_{s}, but we have checked that these extra solutions are always complex, and hence they do not provide anything which could be interpreted as instabilities. This procedure has allowed us to make an exhaustive numerical analysis of the Hopf instabilities for $g \neq 0$, of which we have shown a characteristic example in Fig. 2.

APPENDIX B: EVALUATION OF THE COVARIANCE MATRIX AND THE EFFECTIVE MECHANICAL PARAMETERS

In this section we explain a route to find the covariance matrix of the DOMPO directly from the linearized quantum Langevin equations, (18). We also prove expression (25) for the effective mechanical thermal phonon number and squeezing.

In order to find the covariance matrix V we proceed as follows. First, we find the left eigenvectors of the linear stability matrix. These can be computed as the eigenvectors of its transpose, $\{\mathcal{L}^T \mathbf{w}_j = \lambda_j \mathbf{w}_j\}_{j=1,2,\ldots,6}$, from which we build the matrix $\mathcal{W} = \mathrm{col}(\mathbf{w}_1^T, \mathbf{w}_2^T, \ldots, \mathbf{w}_6^T)$, as well as the diagonal matrix of eigenvalues $\Lambda = \mathrm{diag}(\lambda_1, \lambda_2, \ldots, \lambda_6)$. With these definitions, we have $\mathcal{W}\mathcal{L} = \Lambda\mathcal{W}$. Hence, applying $\mathcal{W}$ on the left-hand side of the linearized Langevin equations, (18), and defining the vector $\hat{\mathbf{c}}(\tau) = \mathcal{W}\delta\hat{\mathbf{b}}(\tau)$, we get a set of uncoupled linear equations for its components, leading to the solution

$$\hat{\mathbf{c}}(\tau) = \sqrt{2}g_{\mathrm{DC}} \int_0^\tau d\tau' e^{\Lambda(\tau-\tau')}\mathcal{W}\hat{\mathbf{f}}(\tau') \qquad (B1)$$

in the asymptotic limit $\tau \gg \max_{j=1,2,\ldots,6} \mathrm{Re}\{\lambda_j\}^{-1}$. It is then straightforward to compute the corresponding correlation matrix $\mathcal{C}$, with elements $C_{jl}(\tau) = \langle \hat{c}_j(\tau)\hat{c}_l(\tau)\rangle$, which, in the asymptotic limit, reads

$$C_{jl} = -2g_{\mathrm{DC}}^2 \frac{(\mathcal{W}\mathcal{M}\mathcal{W}^T)_{jl}}{\lambda_j + \lambda_l}, \qquad (B2)$$

where the matrix $\mathcal{M}$ is defined in (20).

On the other hand, the quadrature vector $\hat{\mathbf{r}}$ is related to the vector $\hat{\mathbf{b}}$ by $\hat{\mathbf{r}} = \mathcal{R}\hat{\mathbf{b}}$, where $\mathcal{R} = \mathcal{R}_{\mathrm{m}} \oplus \mathcal{R}_{\mathrm{p}} \oplus \mathcal{R}_{\mathrm{s}}$, with

$$\mathcal{R}_{\mathrm{m}} = \frac{1}{g_{\mathrm{DC}}}\begin{pmatrix} 1/\sqrt{\Omega} & 0 \\ 0 & \sqrt{\Omega} \end{pmatrix},$$

$$\mathcal{R}_{\mathrm{p}} = \frac{1}{g_{\mathrm{DC}}\sqrt{\kappa}}\begin{pmatrix} 1 & 1 \\ -i & i \end{pmatrix}, \qquad (B3)$$

$$\mathcal{R}_{\mathrm{s}} = \frac{1}{g_{\mathrm{DC}}}\begin{pmatrix} 1 & 1 \\ -i & i \end{pmatrix},$$

and hence, its fluctuations can be written as $\delta\hat{\mathbf{r}}(\tau) = \mathcal{R}\mathcal{W}^{-1}\hat{\mathbf{c}}(\tau)$, leading to the final form of the covariance matrix

in the asymptotic limit

$$V = \mathcal{R}\mathcal{W}^{-1}(\mathcal{C} + \mathcal{C}^T)\mathcal{W}^{-1T}\mathcal{R}^T. \qquad (B4)$$

This is the expression that we have used to compute the Gaussian steady state of the system, which can be efficiently evaluated numerically for any value of the parameters, since it just requires diagonalizing the 6×6 matrix $\mathcal{L}^T$.

Let us now derive the relation between the effective mechanical parameters and the elements of the mechanical covariance matrix. In order to find it, we just need to realize that the thermal state is a Gaussian state with covariance matrix $V_{\mathrm{th}}(\bar{n}_{\mathrm{eff}}) = (2\bar{n}_{\mathrm{eff}} + 1)\mathcal{I}_{2\times 2}$, where $\mathcal{I}_{2\times 2}$ is the 2×2 identity matrix, while the squeezing operator simply acts as the symplectic transformation $\mathcal{S}(r_{\mathrm{eff}}) = \mathrm{diag}(e^{-r_{\mathrm{eff}}}, e^{r_{\mathrm{eff}}})$ in the space of the covariance matrices [15,16]. Hence, the Gaussian state corresponding to (24) has a diagonal covariance matrix:

$$\tilde{V}_{\mathrm{m}}(\bar{n}_{\mathrm{eff}}, r_{\mathrm{eff}}) = \mathcal{S}(r_{\mathrm{eff}})V_{\mathrm{th}}(\bar{n}_{\mathrm{eff}})\mathcal{S}^T(r_{\mathrm{eff}})$$
$$= (2\bar{n}_{\mathrm{eff}} + 1)\mathrm{diag}(e^{-2r_{\mathrm{eff}}}, e^{2r_{\mathrm{eff}}}). \qquad (B5)$$

Therefore, the phase shift $\hat{R}(\theta)$ applied to $\hat{\rho}_{\mathrm{m}}$ in Eq. (24) is nothing but the rotation that diagonalizes V_{m}, turning it into

$$\tilde{V}_{\mathrm{m}} = \mathrm{diag}(V_-, V_+), \qquad (B6)$$

where the eigenvalues of V_{m} are given by $V_\mp = \mathrm{tr}\{V_{\mathrm{m}}\}/2 \mp \sqrt{\mathrm{tr}\{V_{\mathrm{m}}\}^2/4 - \det\{V_{\mathrm{m}}\}}$. In other words, θ is the angle in phase space that captures the direction in which squeezing is applied to the mechanical motion. Matching the expressions, (B5) and (B6), for the diagonal forms of $\tilde{V}_{\mathrm{m}}$ provides the expressions, (25), in the text.

---

[1] R. W. Boyd, *Nonlinear Optics* (Academic Press, New York, 2003).

[2] P. Meystre and D. F. Walls (eds.), *Nonclassical Effects in Quantum Optics* (American Institute of Physics, Melville, NY, 1991).

[3] C. Navarrete-Benlloch, arXiv:1504.05917.

[4] H. J. Carmichael, *Statistical Methods in Quantum Optics 2* (Springer-Verlag, Berlin, 2008).

[5] Y. Takeno, M. Yukawa, H. Yonezawa, and A. Furusawa, Opt. Express **15**, 4321 (2007).

[6] H. Vahlbruch, M. Mehmet, S. Chelkowski, B. Hage, A. Franzen, N. Lastzka, S. Gossler, K. Danzmann, and R. Schnabel, Phys. Rev. Lett. **100**, 033602 (2008).

[7] T. Eberle, S. Steinlechner, J. Bauchrowitz, V. Handchen, H. Vahlbruch, M. Mehmet, H. Muller-Ebhardt, and R. Schnabel, Phys. Rev. Lett. **104**, 251102 (2010).

[8] M. Mehmet, H. Vahlbruch, N. Lastzka, K. Danzmann, and R. Schnabel, Phys. Rev. A **81**, 013814 (2010).

[9] The LIGO Scientific Collaboration, Nat. Phys. **7**, 962 (2011).

[10] K. Goda, O. Miyakawa, E. E. Mikhailov, S. Saraf, R. Adhikari, K. McKenzie, R. Ward, S. Vass, A. J. Weinstein, and N. Mavalvala, Nat. Phys. **4**, 472 (2008).

[11] H. Vahlbruch, S. Chelkowski, B. Hage, A. Franzen, K. Danzmann, and R. Schnabel, Phys. Rev. Lett. **95**, 211102 (2005).

[12] N. Treps, N. Grosse, W. P. Bowen, C. Fabre, H.-A. Bachor, and P. K. Lam, Science **301**, 940 (2003).

[13] N. Treps, U. Andersen, B. Buchler, P. K. Lam, A. Maître, H.-A. Bachor, and C. Fabre, Phys. Rev. Lett. **88**, 203601 (2002).

[14] S. L. Braunstein and P. van Loock, Rev. Mod. Phys. **77**, 513 (2005).

[15] C. Weedbrook, S. Pirandola, R. García-Patron, N. J. Cerf, T. C. Ralph, J. H. Shapiro, and S. Lloyd, Rev. Mod. Phys. **84**, 621 (2012).

[16] C. Navarrete-Benlloch, *An Introduction to the Formalism of Quantum Information with Continuous Variables* (Morgan & Claypool and IOP, Bristol, 2015).

[17] T. J. Kippenberg and K. J. Vahala, Opt. Express **15**, 17172 (2007).

[18] F. Marquardt and S. M. Girvin, Physics **2**, 40 (2009).

[19] P. Meystre, Ann. Phys. **525**, 215 (2013).

[20] M. Aspelmeyer, T. J. Kippenberg, and F. Marquardt, Rev. Mod. Phys. **86**, 1391 (2014).

[21] S. Gigan, H. R. Böhm, M. Paternostro, F. Blaser, G. Langer, J. B. Hertzberg, K. C. Schwab, D. Bäuerle, M. Aspelmeyer, and A. Zeilinger, Nature **444**, 67 (2006).

[22] O. Arcizet, P.-F. Cohadon, T. Briant, M. Pinard, and A. Heidmann, Nature **444**, 71 (2006).

[23] A. Schliesser, P. Del'Haye, N. Nooshi, K. J. Vahala, and T. J. Kippenberg, Phys. Rev. Lett. **97**, 243905 (2006).

[24] T. Corbitt, Y. Chen, E. Innerhofer, H. Müller-Ebhardt, D. Ottaway, H. Rehbein, D. Sigg, S. Whitcomb, C. Wipf, and N. Mavalvala, Phys. Rev. Lett. **98**, 150802 (2007).

[25] J. D. Thompson, B. M. Zwickl, A. M. Jayich, F. Marquardt, S. M. Girvin, and J. G. E. Harris, Nature **452**, 72 (2008).

[26] D. J. Wilson, C. A. Regal, S. B. Papp, and H. J. Kimble, Phys. Rev. Lett. **103**, 207204 (2009).

[27] J. D. Teufel, T. Donner, D. Li, J. W. Harlow, M. S. Allman, K. Cicak, A. J. Sirois, J. D. Whittaker, K. W. Lehnert, and R. W. Simmonds, Nature **475**, 359 (2011).

[28] J. Chan, T. P. Mayer Alegre, A. H. Safavi-Naeini, J. T. Hill, A. Krause, S. Gröblacher, M. Aspelmeyer, and O. Painter, Nature **478**, 89 (2011).

[29] M. Karuza, C. Molinelli, M. Galassi, C. Biancofiore, R. Natali, P. Tombesi, G. Di Giuseppe, and D. Vitali, New J. Phys. **14**, 095015 (2012).

[30] M. Underwood, D. Mason, D. Lee, H. Xu, L. Jiang, A. B. Shkarin, K. Børkje, S. M. Girvin, and J. G. E. Harris, Phys. Rev. A **92**, 061801(R) 2015.

[31] I. Wilson-Rae, N. Nooshi, W. Zwerger, and T. J. Kippenberg, Phys. Rev. Lett. **99**, 093901 (2007).

[32] F. Marquardt, J. P. Chen, A. A. Clerk, and S. M. Girvin, Phys. Rev. Lett. **99**, 093902 (2007).

[33] C. Genes, D. Vitali, P. Tombesi, S. Gigan, and M. Aspelmeyer, Phys. Rev. A **77**, 033804 (2008).

[34] W. Marshall, C. Simon, R. Penrose, and D. Bouwmeester, Phys. Rev. Lett. **91**, 130401 (2003).

[35] D. Kleckner, I. Pikovski, E. Jeffrey, L. Ament, E. Eliel, J. van den Brink, and D. Bouwmeester, New J. Phys. **10**, 095020 (2008).

[36] O. Romero-Isart, A. C. Pflanzer, F. Blaser, R. Kaltenbaek, N. Kiesel, M. Aspelmeyer, and J. I. Cirac, Phys. Rev. Lett. **107**, 020405 (2011).

[37] O. Romero-Isart, Phys. Rev. A **84**, 052121 (2011).

[38] C. Fabre, Phys. Rev. A **49**, 1337 (1994).

[39] S. Mancini and P. Tombesi, Phys. Rev. A **49**, 4055 (1994).

[40] D. W. C. Brooks, T. Botter, S. Schreppler, T. P. Purdy, N. Brahms, and D. M. Stamper-Kurn, Nature **488**, 476 (2012).

[41] A. H. Safavi-Naeini, S. Gröblacher, J. T. Hill, J. Chan, M. Aspelmeyer, and O. Painter, Nature **500**, 185 (2013).

[42] S. Weis, R. Rivière, S. Deléglise, E. Gavartin, O. Arcizet, A. Schliesser, and T. J. Kippenberg, Science **330**, 1520 (2010).

[43] A. H. Safavi-Naeini, T. P. M. Alegre, J. Chan, M. Eichenfield, M. Winger, Q. Lin, J. T. Hill, D. E. Chang, and O. Painter, Nature **472**, 69 (2011).

[44] J. D. Teufel, D. Li, M. S. Allman, K. Cicak, A. J. Sirois, J. D. Whittaker, and R. W. Simmonds, Nature **471**, 204 (2011).

[45] F. Massel, S. U. Cho, J.-M. Pirkkalainen, P. J. Hakonen, T. T. Heikkilä, and M. A. Sillanpää, Nat. Commun. **3**, 987 (2012).

[46] M. Karuza, C. Biancofiore, M. Bawaj, C. Molinelli, M. Galassi, R. Natali, P. Tombesi, G. Di Giuseppe, and D. Vitali, Phys. Rev. A **88**, 013804 (2013).

[47] P. Rabl, Phys. Rev. Lett. **107**, 063601 (2011).

[48] K. Stannigel, P. Rabl, A. S. Sørensen, P. Zoller, and M. D. Lukin, Phys. Rev. Lett. **105**, 220501 (2010).

[49] A. H. Safavi-Naeini and O. Painter, New J. Phys. **13**, 013017 (2011).

[50] C. A. Regal and K. W. Lehnert, J. Phys.: Conf. Ser. **264**, 012025 (2011).

[51] J. M. Taylor, A. S. Sørensen, C. M. Marcus, and E. S. Polzik, Phys. Rev. Lett. **107**, 273601 (2011).

[52] Y.-D. Wang and A. A. Clerk, Phys. Rev. Lett. **108**, 153603 (2012).

[53] Y.-D. Wang and A. A. Clerk, New J. Phys. **14**, 105010 (2012).

[54] Sh. Barzanjeh, M. Abdi, G. J. Milburn, P. Tombesi, and D. Vitali, Phys. Rev. Lett. **109**, 130503 (2012).

[55] J. Bochmann, A. Vainsencher, D. D. Awschalom, and A. N. Cleland, Nat. Phys. **9**, 712 (2013).

[56] T. Bagci, A. Simonsen, S. Schmid, L. G. Villanueva, E. Zeuthen, J. Appel, J. M. Taylor, A. Sørensen, K. Usami, A. Schliesser, and E. S. Polzik, Nature **507**, 81 (2014).

[57] R. W. Andrews, R. W. Peterson, T. P. Purdy, K. Cicak, R. W. Simmonds, C. A. Regal, and K. W. Lehnert, Nat. Phys. **10**, 321 (2014).

[58] A. Schliesser, Ph.D. Thesis, Ludwig-Maximilians-Universität München (2009).

[59] T. A. Palomaki, J. W. Harlow, J. D. Teufel, R. W. Simmonds, and K. W. Lehnert, Nature **495**, 210 (2013).

[60] S. Huang and G. S. Agarwal, Phys. Rev. A **79**, 013821 (2009).

[61] S. Huang and G. S. Agarwal, Phys. Rev. A **80**, 033807 (2009).

[62] V. Peano, H. G. L. Schwefel, Ch. Marquardt, and F. Marquardt, Phys. Rev. Lett. **115**, 243603 (2015).

[63] G. S. Agarwal and S. Huang, arXiv:1602.02214.

[64] X.-Y. Lü, Y. Wu, J. R. Johansson, H. Jing, J. Zhang, and F. Nori, Phys. Rev. Lett. **114**, 093602 (2015).

[65] A. Xuereb, M. Barbieri, and M. Paternostro, Phys. Rev. A **86**, 013809 (2012).

[66] V. S. Ilchenko, A. A. Savchenkov, A. B. Matsko, and L. Maleki, J. Opt. Soc. Am. B **20**, 333 (2003).

[67] V. S. Ilchenko, A. A. Savchenkov, A. B. Matsko, and L. Maleki, Phys. Rev. Lett. **92**, 043903 (2004).

[68] A. A. Savchenkov, A. B. Matsko, M. Mohageg, D. V. Strekalov, and L. Maleki, Opt. Lett. **32**, 157 (2007).

[69] J. U. Fürst, D. V. Strekalov, D. Elser, M. Lassen, U. L. Andersen, C. Marquardt, and G. Leuchs, Phys. Rev. Lett. **104**, 153901 (2010).

[70] J. U. Fürst, D. V. Strekalov, D. Elser, A. Aiello, U. L. Andersen, Ch. Marquardt, and G. Leuchs, Phys. Rev. Lett. **105**, 263904 (2010).

[71] J. Hofer, A. Schliesser, and T. J. Kippenberg, Phys. Rev. A **82**, 031804(R) (2010).

[72] J. U. Fürst, D. V. Strekalov, D. Elser, A. Aiello, U. L. Andersen, Ch. Marquardt, and G. Leuchs, Phys. Rev. Lett. **106**, 113901 (2011).

[73] T. Beckmann, H. Linnenbank, H. Steigerwald, B. Sturman, D. Haertle, K. Buse, and I. Breunig, Phys. Rev. Lett. **106**, 143903 (2011).

[74] C. S. Werner, T. Beckmann, K. Buse, and I. Breunig, Opt. Lett. **37**, 4224 (2012).

[75] M. Förtsch, J. U. Fürst, C. Wittmann, D. Strekalov, A. Aiello, M. V. Chekhova, C. Silberhorn, G. Leuchs, and C. Marquardt, Nat. Commun. **4**, 1818 (2013).

[76] C. Marquardt, D. Strekalov, J. Fürst, M. Förtsch, and G. Leuchs, Opt. Phot. News **24**, 38 (2013).

[77] M. Förtsch, G. Schunk, J. U. Fürst, D. Strekalov, T. Gerrits, M. J. Stevens, F. Sedlmeir, H. G. L. Schwefel, S. W. Nam, G. Leuchs, and C. Marquardt, Phys. Rev. A **91**, 023812 (2015).

[78] M. Förtsch, T. Gerrits, M. J. Stevens, D. Strekalov, G. Schunk, J. U. Fürst, U. Vogl, F. Sedlmeir, H. G. L. Schwefel, G. Leuchs, S. W. Nam, and C. Marquardt, J. Opt. **17**, 065501 (2015).

[79] Z. Leghtas, S. Touzard, I. M. Pop, A. Kou, B. Vlastakis, A. Petrenko, K. M. Sliwa, A. Narla, S. Shankar, M. J. Hatridge, M. Reagor, L. Frunzio, R. J. Schoelkopf, M. Mirrahimi, and M. H. Devoret, Science **347**, 853 (2015).

[80] P. D. Nation, J. Suh, and M. P. Blencowe, Phys. Rev. A **93**, 022510 (2016).

[81] S. Gigan, L. Lopez, V. Delaubert, N. Treps, C. Fabre, and A. Maitre, J. Mod. Opt. **53**, 809 (2006).

[82] L. Lugiato, C. Oldano, C. Fabre, E. Giacobino, and R. J. Horowicz, Nuovo Cimento **10**, 959 (1988).

[83] N. P. Pettiaux, R.-D. Li, and P. Mandel, Opt. Commun. **72**, 256 (1989).

[84] C. Fabre, E. Giacobino, A. Heidmann, L. Lugiato, S. Reynaud, M. Valdacchino, and W. Kaige, Quantum Opt. **2**, 159 (1990).

[85] P. Degenfeld-Schonburg, M. Abdi, M. J. Hartmann, and C. Navarrete-Benlloch, Phys. Rev. A **93**, 023819 (2016).

[86] D. F. Walls and G. Milburn, *Quantum Optics* (Springer, Berlin, 2007).

[87] C. W. Gardiner and P. Zoller, *Quantum Noise* (Springer-Verlag, Berlin, 2004).

[88] L. M. Narducci and N. B. Abraham, *Laser Physics and Laser Instabilities* (World Scientific, Singapore, 1988).

[89] C. Navarrete-Benlloch, E. Roldán, Y. Chang, and T. Shi, Opt. Express **22**, 24010 (2014).

[90] P. D. Drummond, K. J. McNeil, and D. F. Walls, J. Mod. Opt. **28**, 211 (1981).

[91] L. A. Lugiato and G. Strini, Opt. Commun. **41**, 67 (1982).

[92] M. J. Collett and C. W. Gardiner, Phys. Rev. A **30**, 1386 (1984).

[93] P. Kinsler, M. Fernée, and P. D. Drummond, Phys. Rev. A **48**, 3310 (1993).

[94] P. Kinsler and P. D. Drummond, Phys. Rev. A **52**, 783 (1995).

[95] P. D. Drummond, K. Dechoum, and S. Chaturvedi, Phys. Rev. A **65**, 033806 (2002).

[96] S. Chaturvedi and P. D. Drummond, Eur. Phys. J. B **8**, 251 (1999).

[97] D. T. Pope, P. D. Drummond, and W. J. Munro, Phys. Rev. A **62**, 042108 (2000).

[98] C. J. Mertens, T. A. B. Kennedy, and S. Swain, Phys. Rev. Lett. **71**, 2014 (1993).

[99] C. J. Mertens, T. A. B. Kennedy, and S. Swain, Phys. Rev. A **48**, 2374 (1993).

[100] O. Veits and M. Fleischhauer, Phys. Rev. A **55**, 3059 (1997).

[101] P. Degenfeld-Schonburg, C. Navarrete-Benlloch, and M. J. Hartmann, Phys. Rev. A **91**, 053850 (2015).

[102] P. D. Drummond and C. W. Gardiner, J. Phys. A: Math. Gen. **13**, 2353 (1980).

[103] P. Degenfeld-Schonburg and M. J. Hartmann, Phys. Rev. B **89**, 245108 (2014).

[104] A. Mari and J. Eisert, Phys. Rev. Lett. **108**, 120602 (2012).